Mechanical adhesion of SiO_2 thin films onto polymeric substrates

C. Ho [a,b], J. Alexis[a], O. Dalverny[a], Y. Balcaen[a], A. Dehoux[b], S. Châtel[b] and B. Faure[b]

[a]Laboratoire Génie de Production INPT-ENIT, University of Toulouse, Tarbes, France; [b]Thin Films Group, R&D Physico-Chemistry, Essilor International, Créteil, France

ABSTRACT

Quantification of adhesion between a 200 nm silicon dioxide layer and a 4.5 µm thick polymeric coating was performed by analysing the SiO_2 buckle morphologies generated under compressive stress. Impacts of mechanical properties of SiO_2 layers, as well as a surface pretreatment on adhesion, are shown. Interfacial toughness of both configurations are assessed using the Hutchinson and Suo model, which involves buckle dimensions determined *in situ* by an optical profilometer, and elastic modulus E_f, of the SiO_2 thin films, characterised by nanoindentation. The surface pretreatment led to initiation of buckling at a higher strain. The same trend is observed for a layer with a lower stiffness and residual stress.

KEYWORDS

Oxide thin film; polymer substrate; mechanical properties; adhesion

Introduction

Besides its main function of providing vision correction, ophthalmic lenses offer additional benefits, such as anti-scratch and anti-reflective properties, in order to optimise visual comfort. These features are brought by coatings deposited on top of the plastic polymeric substrate constituting the lens. More specifically, an anti-scratch hard coat of a few microns thick is deposited by wet chemical methods, followed by the evaporation of an anti-reflective stack within the nanometric scale. The challenge is to ensure interface quality between layers. Considering their small dimensions, assessment of mechanical adhesion within the stack is mostly performed qualitatively to this day. The aim of this research is to provide a quantitative estimate of the mechanical adhesion at the most sensitive interface of the structure, located between the SiO_2 thin film and the hard coat. Among the 300 adhesion tests described in the literature, several methods have been implemented to study the adhesion of rigid thin films on soft substrates such as scratch tests, tensile tests and interfacial indentation tests [1–5]. The chosen method should not only allow ranking of adhesion but also give information on critical interfacial stresses or even adhesion energy. Considering these requirements and preliminary testing, compression tests appear to be the most promising for characterising our structure. Buckling morphologies generated by compressive stress are often used to characterise metallic thin films on polymeric substrates [6–9]. Few authors have applied compression adhesion tests to non-metallic thin films. Abdallah et al. studied buckle morphologies of 400 nm thick Si_3N_4 deposited on a hard coat on top of AcryLite™ substrate [10]. Evaluation of the interfacial properties of an oxide thin film deposited on a polymeric substrate by compression tests has not yet been reported and therefore sets the framework for this research. In this study, we present the results of adhesion characterisation of 200 nm SiO_2 thin films on polymeric substrates under compressive stress and provide quantitative estimates of interface quality. Difference in adhesion between coatings can be explained by the surface pretreatment, mechanical properties of layers, such as their stiffness or residual stress.

Materials and methods

The multilayer system under study

SiO_2 thin films were deposited by evaporation under vacuum on top of a standard ophthalmic structure. This particular ophthalmic structure consists of a 4.5 µm thick composite polymer, referred to as a hard coat, on a 4 mm thick polycarbonate substrate. Depositions of three types of SiO_2 layers were conducted at a pressure of 8×10^{-5} to 1.5×10^{-4} mbar, which is similar to the procedure used by Roisin and Thomas [11]. SiO_2 Type A and B are resulting from different gas supply conditions during deposition; no surface pre-treatment was applied before deposition. SiO_2 Type A is deposited along with oxygen gas, whereas SiO_2 Type B deposition does not involve the introduction of an additional gas. This difference in processing has been shown to effectively generate different levels of residual stress within the SiO_2 layers because gas scattering during deposition increases porosity [12]. SiO_2 Type C was deposited under the same conditions as SiO_2 Type B but received a surface

CONTACT J. Alexis joel.alexis@enit.fr

pretreatment before deposition consisting of an ionic pre-cleaning by argon ion bombarding [11,13–15].

Compressive test experimental setup

Compression stage

The configurations of SiO_2 Type A, B, and C on a lens structure were tested. Micro-compression tests were performed on a Deben stage with a 5 kN load cell under compression mode. The motor speed was set to 0.2 mm min^{-1}. Buckling phenomena were observed and recorded using a Wyko NT1100 optical profilometer. Video extensometer was used to estimate true strain in the substrate to generate buckling. Slenderness calculations were made to define the geometries of compressed beams to avoid buckling of the substrate [16]. Calculated slenderness was then compared to the critical slenderness λ_c.

$$\lambda_c = \pi\sqrt{\frac{E}{R_e}} \tag{1}$$

where E is the elastic modulus of the polycarbonate substrate and R_e is its yield strength. The elastic modulus of the polycarbonate and yield strength were determined to be 1872 and 80 MPa, respectively, which gives a critical slenderness of 15. For a sample dimension of $5 \times 15 \times 4$ mm^3, $\lambda < \lambda_c$, therefore buckling of the substrate is not expected.

Development of the test protocol

Inhomogeneity of deformation can occur due to friction between the sample and clamping jaws. To determine the homogeneity of the examined surface, a finite element model of the macroscopic polycarbonate substrate was built. A three-dimensional quasi-static mechanical model was used to simulate a full sample with infinite friction with the clamping jaws. The polycarbonate substrate was modelled with an elasto-plastic law ($E = 1.8$ GPa, $\nu = 0.37$, $\sigma_y = 80$ MPa). A boundary displacement along the y-axis was used as the load and was applied to the top face while the bottom face remained clamped. This boundary condition represents the most unfavourable case regarding strain homogeneity in the observation area. Part of the model was meshed with 20-node quadratic brick with reduced integration elements (C3DR20 in Abaqus® FEM software). The results of the numerical model give a deviation from homogeneity of strain of 0.1% within the area of interest for a 5.0% applied strain (Figure 1). Because the stress state is sufficiently homogeneous, we could expect a regular distribution of buckles in the region being observed.

The strain field in the polycarbonate substrate subjected to uniaxial compressive deformation was also studied by digital image correlation using 2M cameras coupled with ARAMIS software. A subset of 20 pixels with a step of 10×10 pixels is chosen. The strain field within the area of interest is marked in grey and is determined to be $4.8 \pm 0.3\%$ at the strain level necessary to study buckling phenomenon (Figure 2), which is on the same order of magnitude as the numerical results. The small calculated standard deviations (0.3%) indicate strain homogeneity of 94% in the observation area.

The observation area under the optical profilometer is 1.8×2.4 mm^2, which is similar to the area studied, therefore providing a strain homogeneity close to 94%.

Analytical model for straight-sided buckles

The analytical model is derived from studying linear elastic fracture mechanics of the buckling of a perfect rectangular plate. The Hutchinson model was improved upon by Griffith's crack propagation criterion, which took mode-mixity into account [17]. The critical compressive biaxial stress at the onset buckling (σ_{B0}) is calculated as follows:

$$\sigma_{B0} = \frac{\pi^2}{12}\frac{E_f}{(1-\nu^2)}\left(\frac{h}{b}\right)^2 \tag{2}$$

where h is the thickness of the film, b is half the width of the buckle and E_f is the plane strain modulus of the film and ν its Poisson's ratio [18]. The energy release rate (G) along the sides of the buckle can be estimated by studying the average energy per area in the unbuckled state (U_0) or the average energy per area in the buckled state (U), which are related by the following equation: $G = U_0 - U$. Expressed differently,

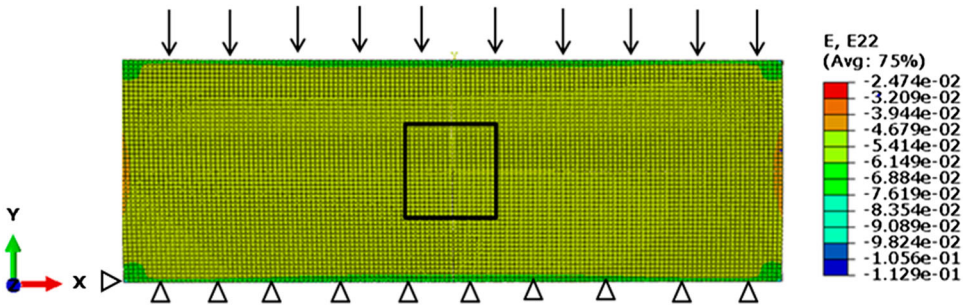

Figure 1. Strain along the compression axis at deformation scale factor of 1 (arrows represent the direction of applied displacement, triangles represent the clamping condition of bottom face and rectangle represents an area of interest).

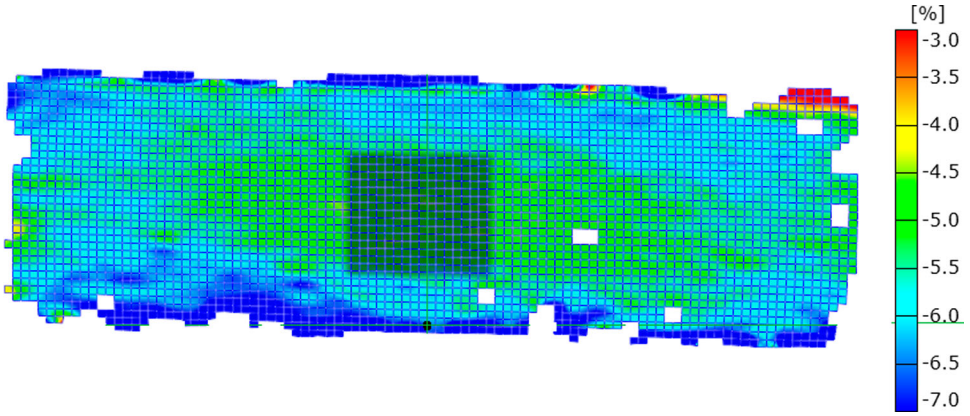

Figure 2. Digital Image Correlation measured of strain homogeneity during a compression test. Maximum variation in the observation area, marked in grey, reaches 0.2%.

the energy release rate (G) is the energy needed per area to separate SiO_2 thin film from substrates over the width of the buckle, and this relationship is defined by the following equation:

$$G = G_0\left(1 - \frac{\sigma_{B0}}{\sigma_r}\right)^2 \tag{3}$$

where G_0 is the available energy per area stored in the unbuckled film. G_0 is given by Equation (5).

$$G_0 = \frac{(1-\nu_f^2)\sigma_r^2 h}{2E_f} \tag{4}$$

where σ_r is the residual stress in the buckled plate, which is given by Equation (6).

$$\sigma_r = \frac{3}{4}\sigma_{B0}\left(\frac{\delta^2}{h^2} + 1\right) \tag{5}$$

where δ is the height of the buckle.

Localisation of delamination was performed using a Hitachi S-3400 N Scanning electron microscope coupled with energy dispersive X-ray (EDS) analysis. The buckle dimensions were determined using a Wyko NT1100 optical profilometer.

Results

Phenomenological aspects

For SiO_2 Type A, initiation, and propagation of buckles was observed during the application of compressive stress on the sample, after a strain of 3.1 ± 0.8%, averaged over three samples, is reached. Buckle width progressively widens with an increase of loading until its degradation, often caused by transverse cracks appearing on the buckle (Figure 3). For SiO_2 Type B on the lens, a strain of 2.1 ± 0.4% was sufficient to see the emergence of buckle morphologies. Similar scenario was observed with buckle growth followed by degradation with an increase of strain. Buckle density steadily increases after instantaneous appearance of the

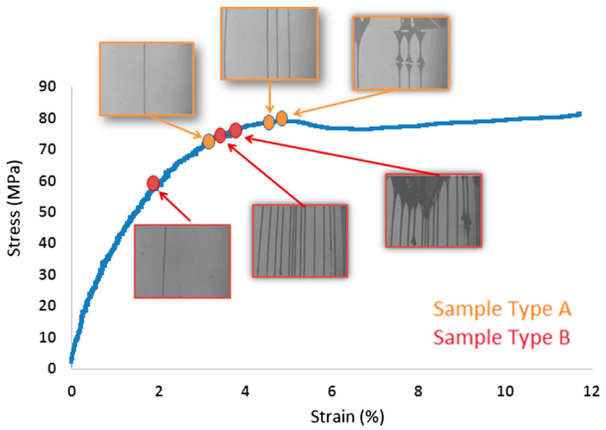

Figure 3. Initiation and evolution of buckles with an increase of strain. The initiation marks the emergence of the first buckle while the evolution pictured represents the strain at which calculations of energy release rates are performed, before degradation of buckles.

first buckle, with a number of buckles significantly higher than that of SiO_2 Type A. For SiO_2 Type C, average initiation strain was 3.4 ± 0.4% and followed an identical sequence of events as SiO_2 Type B.

During the unloading phase, a progressive conversion from straight-sided buckles into telephone cord morphologies was observed (Figure 4). The occurrence of telephone cords during unloading is common and is consistent with the stability diagram of unilateral buckling patterns established by Parry et al. [18–20].

Identification of delaminated interface

A layer containing buckles has been identified in a specimen where buckles have been removed by tape to release the interface. The step height of the delaminated areas identified with AFM was found to be 200 nm, which corresponds to the thickness of the SiO_2 layer. Profile analysis of the chemical composition of a delaminated area shows that in the lower zones, the quantity of silicon and oxygen are lower and the quantity of carbon is higher (Figure 5). These analyses

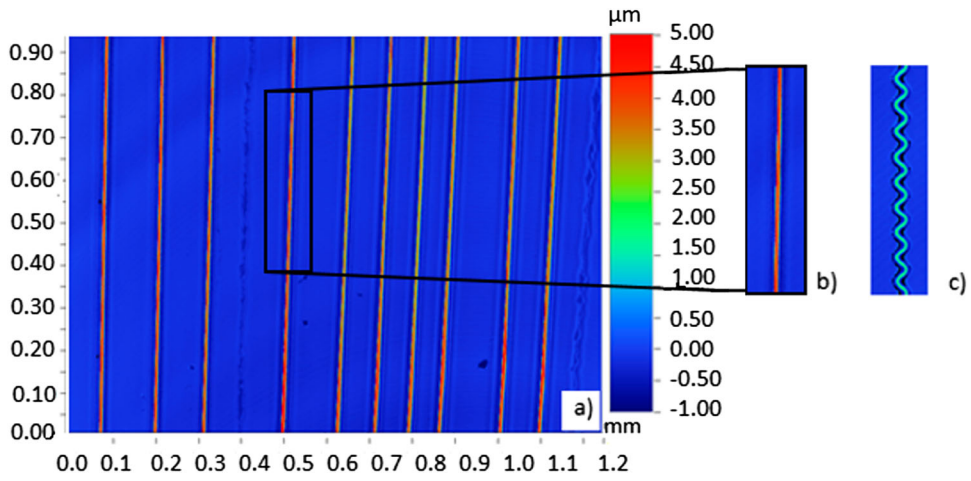

Figure 4. (a) Example of buckles observed for SiO_2 Type B, (b) example of a buckle and its evolution to a telephone cord after unloading of sample (c).

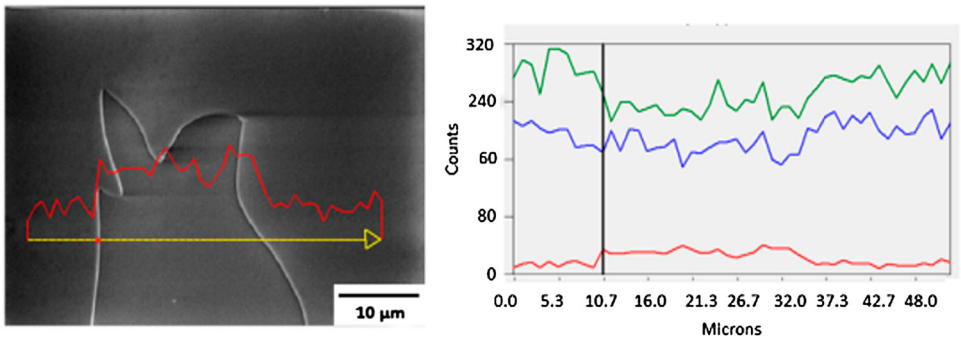

Figure 5. EDS characterisation of a delaminated area (Carbon: Bottom curve, Silicon: Middle curve and Oxygen: Upper curve).

strongly suggest delamination at the SiO_2/hard coat interface and validate the micro-compressive test as an effective technique for acquiring information on the adhesion at the interface of interest.

Quantification of adhesion

The total number of buckles measured on three different samples per configuration is, respectively, 9, 31 and 23 for sample type A, B and C. Width and height of buckles are measured at a strain before degradation of buckles, that is a strain of 4.5% for sample A, 3.3% for sample B and 4.9% for sample C. Calculated energy release rates using Hutchinson and Suo model range from 0.1 to 1 J m^{-2} for SiO_2 Type A, 1.5 to 3.5 J m^{-2} for SiO_2 Type B and from 1.7 to 3 J m^{-2} for SiO_2 Type C , which is in the same order of magnitude as adhesion energies found in the literature; for example, 1.9 to 2.7 J m^{-2} for Tungsten-Titanium (WTi) film on borophosphosilicate glass (BPSG) substrates or 4.3 to 6.3 J m^{-2} for ITO layers on Hard coat on Acrylite substrate [21,22].

Discussion

Difference in initiation strain between samples B and C should be mainly linked to surface pre-treatment since both layers were deposited under the same conditions. However, difference in response between samples A and B after the application of compressive stress, do not seem to result from variation of surface treatment since both configurations underwent similar preparation process. It had been shown in the literature that deposition conditions such as additional gas during evaporation could affect the mechanical properties of layers [12]. Therefore, we are focusing on determining residual stress and elastic modulus for SiO_2 Type A and B; mechanical properties of SiO_2 Type C being assumed identical to that of SiO_2 Type A.

Compressive residual stresses of SiO_2 Type A and B were evaluated using specific bi-metallic glass strips (60 mm × 50 mm × 150 µm) and the equation developed by Stoney [23,24].

$$\sigma_s = -E_s \frac{h_s^2}{(1-\nu_s)h_f}\frac{1}{R} \tag{6}$$

Table 1. Elastic moduli of SiO_2 Type A and B deposited ophthalmic lens, using the Hay and Crawford model.

Substrate	Young's Modulus (GPa) SiO_2 A	Young's Modulus (GPa) SiO_2 B
Hard coat on Polycarbonate	33 ± 1	50 ± 0

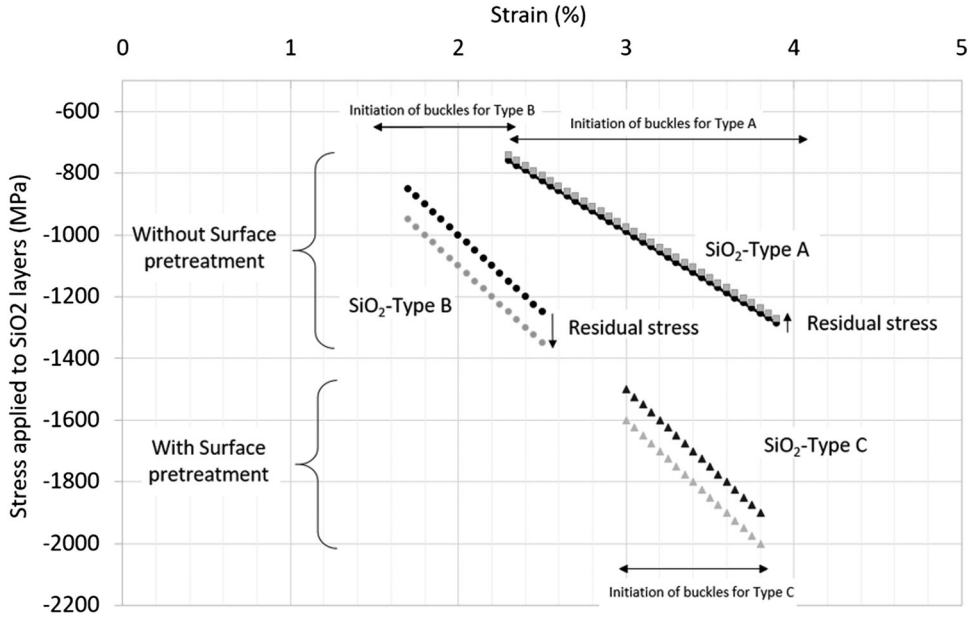

Figure 6. Stress applied to SiO_2 layers as a function of strain. Grey and black marks represent with and without residual stress taken into account, respectively.

where E_s is Young's modulus of the substrate; h_s and h_f are the substrate and film thickness, respectively; ν_s is the Poisson's ratio of the substrate, and R is the radius of curvature. The compressive residual stresses were estimated to be roughly +16 and −100 MPa, respectively for SiO_2 type A and B.

The Young's moduli of the two sample configurations were characterised with a Nanoscope XP III from MTS using continuous stiffness mode with a DCM measuring head and Berkovich diamond tip. A matrix of 30 indents separated by 30 µm was created for each configuration. The elastic modulus of the hard coat was measured to be between 6 and 7 GPa by nanoindentation using the model developed by Oliver and Pharr between 20 and 30 nm [25]. Moduli of SiO_2 thin films are highly dependent on substrate; thus, Hay and Crawford's model was used to take into account the influence of the substrate (Table 1) [26]. This model has been chosen because of its applicability for soft substrates within $E_f/E_s < 10$, which is in line with the configurations on polymeric substrate.

As seen before, difference of strain threshold for initiation of buckling phenomenon shows SiO_2 type B's suitability with regard to buckling. This could be explained by a higher elastic mismatch between film and substrate that can make it easier for the film to buckle when strain is applied, leading to a lower strain for initiation.

Moreover, higher compressive residual stress in SiO_2 Type B after deposition can add up to compressive stress applied during the experiments to reach the stress threshold for interfacial debonding faster (Figure 6). Finally, the debonding stress seems identical for the SiO_2 Type A and B, which is consistent with the fact that surface pretreatment is similar.

As said previously, SiO_2 Type C underwent a similar deposition process as SiO_2 Type B resulting in identical mechanical properties, that is, a higher stiffness and residual stress compared to SiO_2 Type A. Therefore, the difference in stress threshold required for debonbing between SiO_2 Type B and C could directly be attributed to surface pretreatment. As we can see in Figure 6, the range of debonding stress between SiO_2 Type B and C is dissimilar, with an average decohesion value at a compressive stress of 1.1 and 1.8 GPa, for layers without and with surface pretreatment, respectively. This suggests that surface pre-treatment allows the interface to withstand an additional 700 MPa compressive stress before fracturing.

Conclusion

Calculated energy release rates are compatible with bibliographical results. It ranges from 0.1 to 1 J m^{-2} for the SiO_2 layer deposited with oxygen (Type A), 1.5 to 3.5 J m^{-2} for the SiO_2 deposited without oxygen (Type B) and from 1.7 to 3 J m^{-2} for the layer deposited after an ionic pre-cleaning by argon ion bombarding (Type C). Future work consists of simulating the adhesion test by compression for a better analysis of fracture energies with plastic dissipation and local strain taken into account.

Acknowledgments

The authors would like to acknowledge P. Calba's Materials Advanced Characterisation team at Essilor International for their technical support.

Disclosure statement

No potential conflict of interest was reported by the authors.

Funding

This research was supported by the ANRT funding under CIFRE - Essilor International partnership.

ORCID

C. Ho http://orcid.org/0000-0002-0514-6426

References

[1] Mittal K. Adhesion measurement of films and coatings: a commentary. In: Mittal KL, editor. Adhesion measurement of films and coatings. Utrecht: VSP (Brill Academic Publishers); 1995. p. 1–13.

[2] Gunda M, Kumar P, Katiyar M. Review of mechanical characterization techniques for thin films used in flexible electronics. Crit Rev Solid State Mater Sci. 2017;42(2):129–152.

[3] Fateh R, Dillert R, Bahnemann D. Preparation and characterization of transparent hydrophilic photocatalytic TiO_2/SiO_2 thin films on polycarbonate. Langmuir. 2013;29(11):3730–3739.

[4] Yang B, Zhang K, Chen G, et al. Measurement of fracture toughness and interfacial shear strength of hard and brittle Cr coating on ductile steel substrate. Surf Eng. 2008;24(5):332–336.

[5] Hadad M, Marot G, Démarécaux P, et al. Adhesion tests for thermal spray coatings: correlation of bond strength and interfacial toughness. Surf Eng. 2007;23 (4):279–283.

[6] Xue X, Wang S, Zeng C, et al. Buckling delamination and cracking of thin titanium films under compression: experimental and numerical studies. Surf Coat Technol. 2014;244:151–157.

[7] Cordill M, Glushko O, Kreith J, et al. Measuring electro-mechanical properties of thin films on polymer substrates. Microelectron Eng. 2014;137:96–100.

[8] Jia H, Wang S, Goudeau P, et al. Investigation of buckling transition from straight-sided to telephone-cord wrinkles in Al films. J Micromech Microeng. 2013;23:045014.

[9] Sun Y, Chen Q, Feng Y, et al. Buckling morphologies and interfacial properties of silicon nitride films deposited on float glass substrates. Surf Rev Lett. 2015;22 (4):1550046.

[10] Abdallah A, Kozodaev D, Bouten P, et al. Buckle morphology of compressed inorganic thin layers on a polymer substrate. Thin Solid Films. 2006;503:167–176.

[11] Roisin P, Thomas M. Method for producing an optical article coated with an antireflection or a reflective coating having improved adhesion and abrasion resistance properties, US 8318245 B2. 2012.

[12] Scherer K, Nouvelot L, Lacan P, et al. Optical and mechanical characterization of evaporated SiO2 layers. Appl Opt. 1996;35(25):5067–5072.

[13] Schulz U, Munzert P, Kaiser N. Plasma surface modification of PMMA for optical applications. J Adhes Sci Technol. 2010;24(7):1283–1289.

[14] Liston E, Martinu L, Wertheimer M. Plasma surface modification of polymers for improved adhesion: a critical review. J Adhes Sci Technol. 1993;7 (10):1091–1127.

[15] Munzert P, Praefke C, Schulz U, et al. Adhesion of vacuum deposited optical coatings on PMMA and polycarbonate. J Adhes Sci Technol. 2012;26 (18-19):2269–2276.

[16] Fanchon J. Guide des sciences et technologies industrielles [guide to science and industrial technologies]. Paris (FR): Nathan; 2016.

[17] Hutchinson J, Suo Z. Mixed mode cracking in layered materials. Adv Appl Mech. 1991;29:63–191.

[18] Moon M, Lee K, Oh K, et al. Buckle delamination on patterned substrates. Acta Mater. 2004;52 (10):3151–3159.

[19] Ni Y, Yu S, Jiang H, et al. The shape of telephone cord blisters. Nat Commun. 2017;8:14138.

[20] Parry G, Cimetière A, Coupeau C, et al. Stability diagram of unilateral buckling patterns of strip-delaminated films. Physical Review E. 2006;74(6):66601.

[21] Kleinbichler A, Zechner J, Cordill MJ. Buckle induced delamination techniques to measure the adhesion of metal dielectric interfaces. Microelectron Eng. 2017;167:63–68.

[22] Abdallah A, Bouten P, de With G. Experimental study on buckle evolution of thin inorganic layers on a polymer substrate. Eng Fract Mech. 2010;77:2896–2905.

[23] Stoney G. The tension of metallic films deposited by electrolysis. Proc R Soc A: Math Phys Eng Sci. 1909;82(553):172–175.

[24] Mallik A, Ray B. Residual stress and nanomechanical properties of sonoelectrodeposited Cu films. Surf Eng. 2011;27(7):551–556.

[25] Oliver W, Pharr G. Improved technique for determining hardness and elastic modulus using load and displacement sensing indentation experiments. J Mater Res. 1992;7(6):1564–1583.

[26] Hay J, Crawford B. Measuring substrate-independent modulus of thin films. J Mater Res. 2011;26 (06):727–738.